Supporting Information

Manipulating defects simultaneously boosts crystal structure stability and the electrochemical reversibility toward long-life aqueous zinc ion batteries

Shuyue Hou, Xinyue Chen, Gangguo He, Xin Peng, Jingjing Wang, Can Huang, Huan Liu, Tiezhong Liu, Xin Wang, Shuang Hou, Lingzhi Zhao**

Mrs. S. Hou, Mrs. X. Chen, Mr. G. He, Mr. X. Peng, Mrs. J. Wang, Mr. C. Huang, Dr. T. Liu, Dr. S. Hou, Prof. L. Zhao

Guangdong Provincial Engineering Technology Research Center for Low Carbon and Advanced Energy Materials, Guangdong Provincial Key Laboratory of Chip and Integration Technology, School of Semiconductor Science and Technology, South China Normal University, Foshan 528225, China

**Corresponding authors E-mail: shou@m.scnu.edu.cn (S. Hou); lzzhao@scnu.edu.cn (L. Zhao)*

Prof. X. Wang

Institute of Carbon Neutrality, Zhejiang Wanli University, Ningbo 315100, China

Mrs. H. Liu

Guangdong Haomei New Materials Co., Ltd, Qingyuan, 511540, China

Experimental section

1. Synthesis of V_2O_5

All reagents were purchased from Aladdin or Macklin and used without further purification. The commercial divanadium pentaoxide (V_2O_5, 6 mmol) was uniformly suspend in deionized water (36 mL) at 75℃, then oxalic acid ($C_2H_2O_4$, 18 mmol) was added and stirred for 2 hours to obtained the ultramarine solution. Next, the above solution was dried at 70℃ for three days to obtain ultramarine solid. Finally, orange V_2O_5 was obtained after calcination in air at 260℃ for 3 h under a heating rate of 2℃ min^{-1}.

2. Synthesis of SVO-1, SVO-2, SVO-3 and SVO-4

In a typical procedure, the above obtained V_2O_5 (0.1 g) and sulfur powder (0.0125 g) were separately placed in a covered porcelain boat, and the sulfur powder was placed on the upstream side in a tubular furnace. Then, the samples were heated at 450℃ for 1 h under a ramping rate of 2℃ min^{-1} in N_2 atmosphere.

When the mass ratio of sulfur to V_2O_5 are 1:8, 1: 6 and 1: 4, the sulfurized products possess heterojunction structures, named as SVO-1, SVO-2, SVO-3 respectively. When the mass ratio of sulfur to V_2O_5 is 1: 1, single-phase VO_2 is obtained, named as SVO-4.

3. Materials characterization

Crystallographic phases were investigated on X-ray powder diffraction (XRD, Ultima IV) using Cu Kα radiation with a scanning speed of 5° min^{-1}. The X-ray photoelectron spectroscopy was tested on Thermo Scientific K-Alpha for analyzing chemical state of elements on the surface of sample. Raman spectroscopy used a laser confocal Raman microscope (Raman, inVia) with a 532 nm laser. The morphology and the detailed crystal structure of the samples were characterized by scanning electron microscopy (SEM. Zeiss Sigma 300) and the transmission electron microscopy (TEM, FEI Talos F200X). The content of sulfur in the sample was measured using an inductively coupled plasma mass spectrometry (ICP-MS, Agilent 7700). The change of crystal structure during the reaction was studied by in-situ XRD (Empyrean, PANalytical).

4. Electrochemical measurement

The electrochemical performances of the samples were determined by assembling a CR2032 coin-type cell. The cathodes were prepared by coating a slurry mixed active materials (V_2O_5, SVO-1, SVO-2, SVO-3, SVO-4), conductive super P, and poly-vinylidene fluoride (PVDF) onto stainless steel-wire mesh (400 mesh) with a mass ratio of 7: 2: 1. A glass-fiber filter paper was used as a separator, zinc-metal foil as a counter electrode, 2 M $Zn(CF_3SO_3)_2$ and 0.07 M sodium dodecyl sulfate (SDS) solution as electrolyte. The galvanostatic charge and discharge (GCD) tests were performed on multi-channel battery testing system (Netware CT4008 and LANHE CT3002A). Cyclic voltammetry (CV) curves (0.2-1.6 V) were obtained by CHI660E electrochemistry workstation, and in situ EIS tests were recorded using a VersaSTAT 3 electrochemistry workstation.

5. DFT Calculation

The Vienna Ab Initio Package (VASP) have been employed to perform all the density functional theory (DFT) calculations within the generalized gradient approximation (GGA) using the PBE formulation. [1-3] The projected augmented wave (PAW) potentials have been chosen to describe the ionic cores and take valence electrons into account using a plane wave basis set with a kinetic energy cutoff of 500 eV. [4, 5] Partial occupancies of the Kohn-Sham orbitals were allowed using the Gaussian smearing method and a width of 0.1 eV. The electronic energy was considered self-consistent when the energy change was smaller than 10^{-5} eV. A geometry optimization was considered convergent when the force change was smaller than 0.05 eV/Å. Grimme's DFT-D3 methodology was used to describe the dispersion interactions.[6]

The equilibrium lattice constants of VO_2 and V_6O_{13} unit cell were optimized, when using a 15×15×3 Monkhorst-Pack k-point grid for Brillouin zone sampling. We then use it to construct a VO_2 (011) and V_6O_{13} (003) surface model with periodicity in the x and y directions and in the z direction seperated by a vacuum layer in the depth of 20 Å in order to separate the surface slab from its periodic duplicates. The formation energy per atom (E_f) of a compound was defined by the dopant: $E_f = E_{total}-N_V\mu_V-N_S\mu_S-N_O\mu_O$. Where E total is the total DFT energy of a given structure, and μ {V,O,S} are the chemical potentials of the constituent atomic species, n{V,O,S} are the number of the constituent atomic species. Finally, transition states for elementary reaction steps were determined by the nudged elastic band (NEB) method.[7] In the NEB method, the path between the reactant and product is discretized into a

series of structural images.

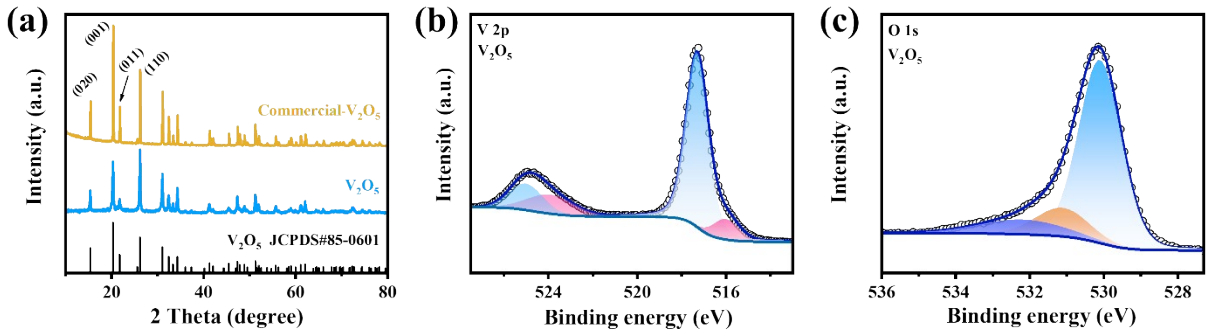

Figure S1. (a) XRD patterns of commercial V_2O_5 and V_2O_5. (b) V 2p, (c) O 1s spectra of V_2O_5.

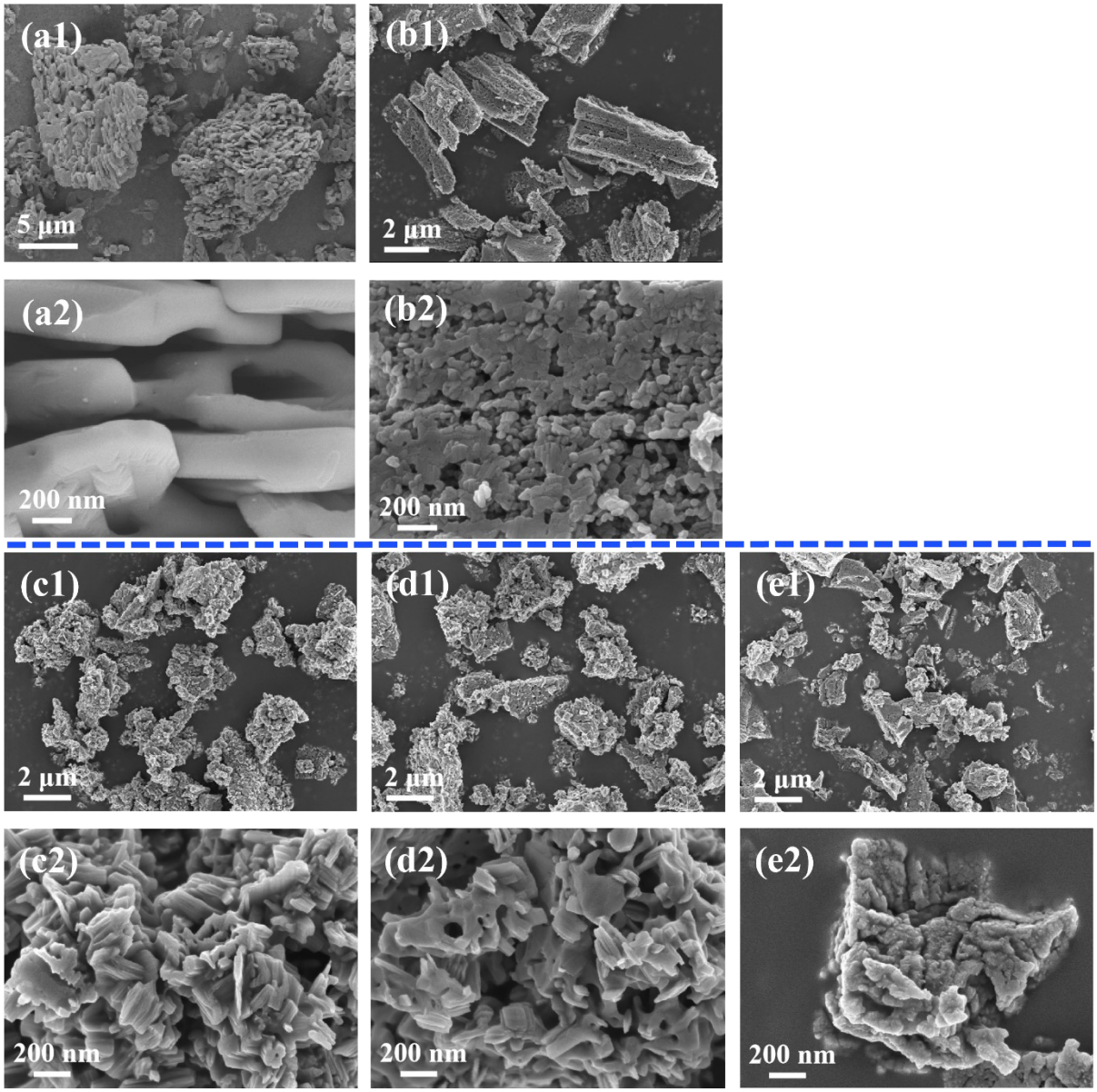

Figure S2. SEM images of (a) commercial V_2O_5, (b) V_2O_5, (c) SVO-1, (d) SVO-3, (e) SVO-4.

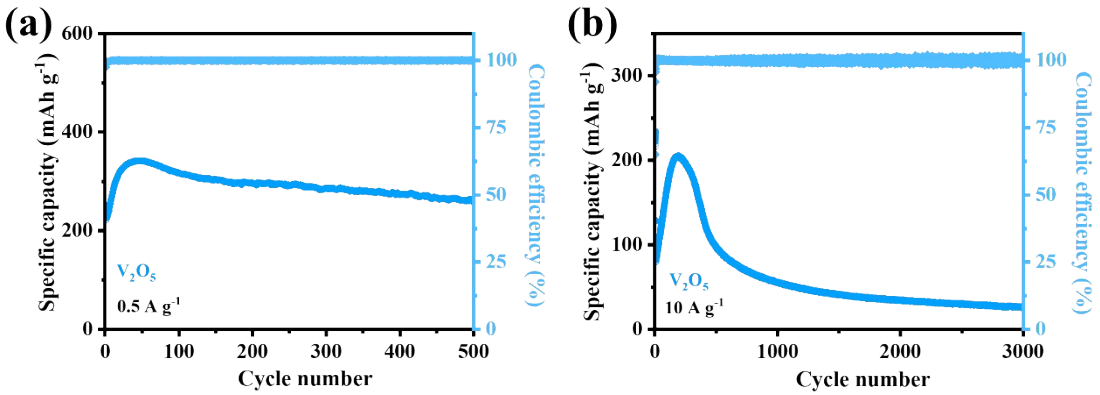

Figure S3. Cycle performance of V_2O_5 at (a) 0.5 A g^{-1} and (b) 10 A g^{-1}.

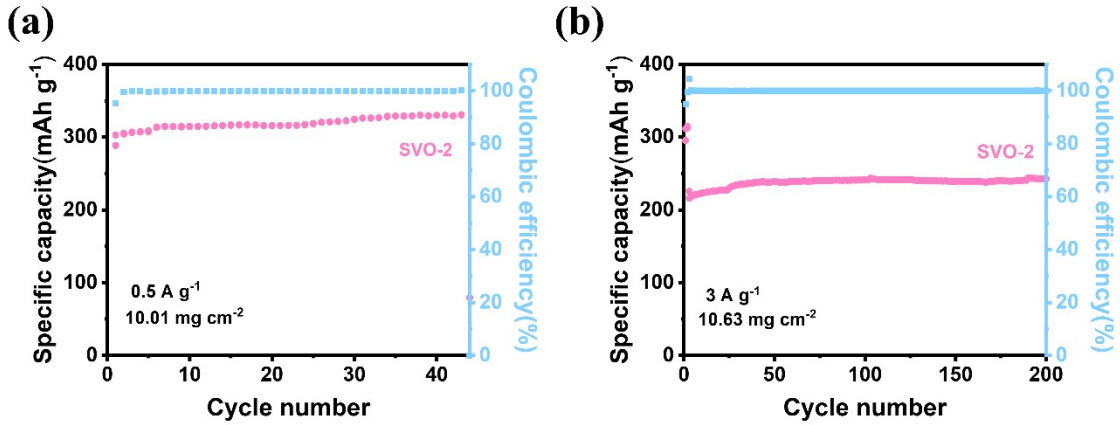

Figure S4. Cycle performance of SVO-2 at high mass loading under (a) 0.5 A g^{-1}; (b) 3 A g^{-1}.

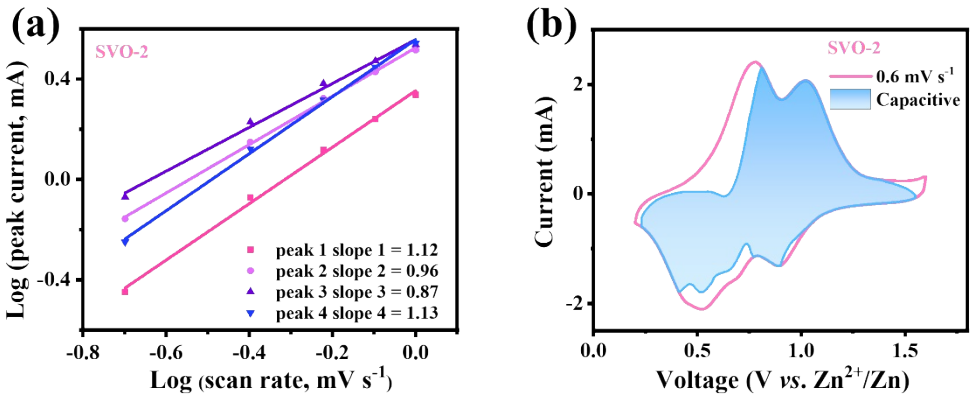

Figure S5. (a) Fitting plots of log(*i*) and log(*v*); (b) Capacitive contribution under 0.6 mV s^{-1}.

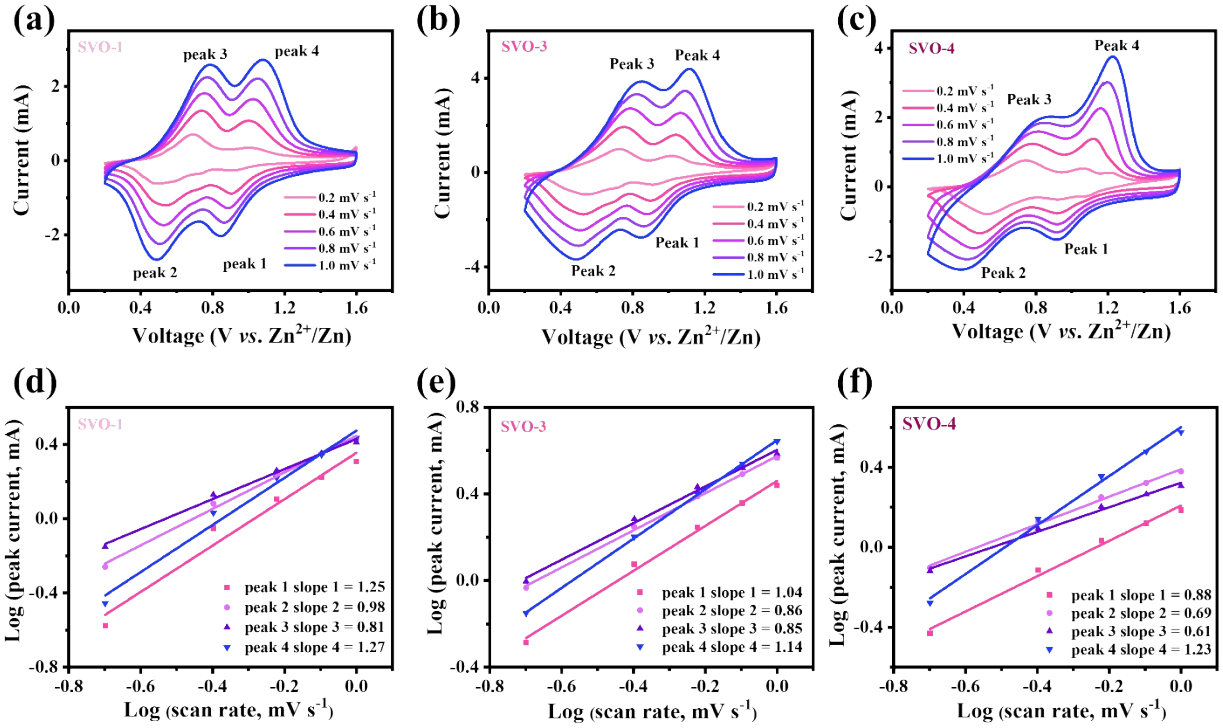

Figure S6. (a-c) CV curves at various scan rates and (d-f) log(*i*) versus log(*v*) plots of the SVO electrodes.

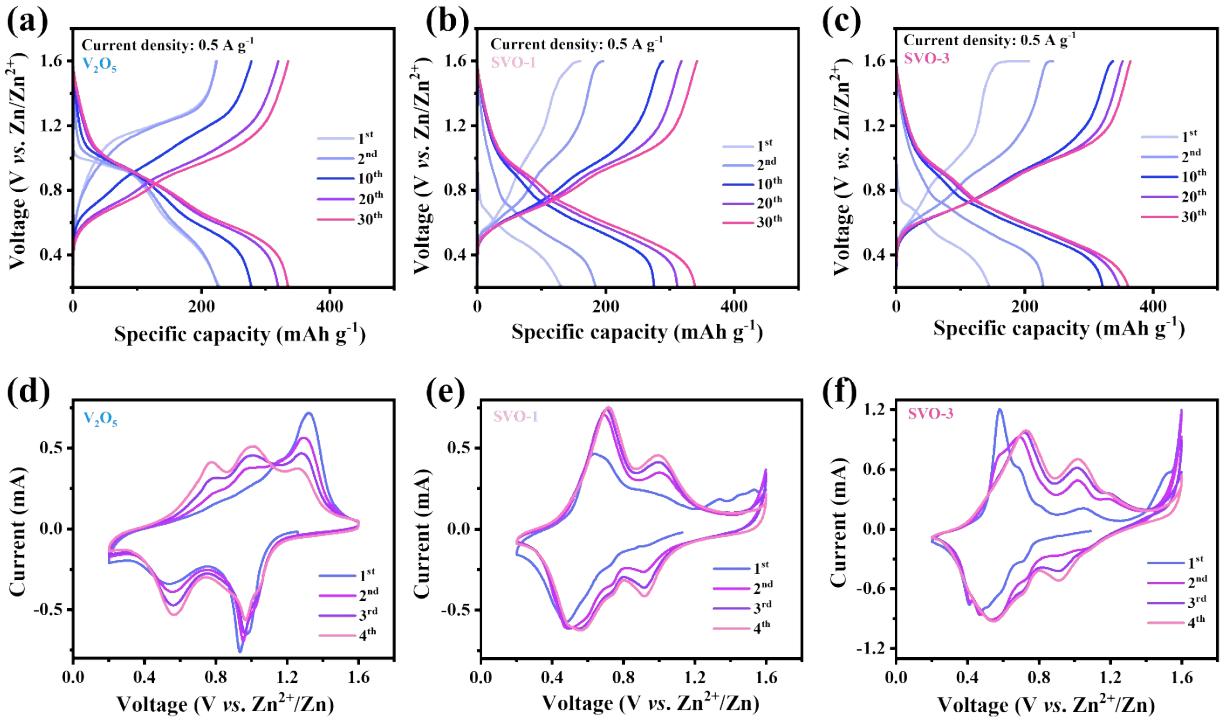

Figure S7. GCD profiles and CV curves of V_2O_5, SVO-1 and SVO-3.

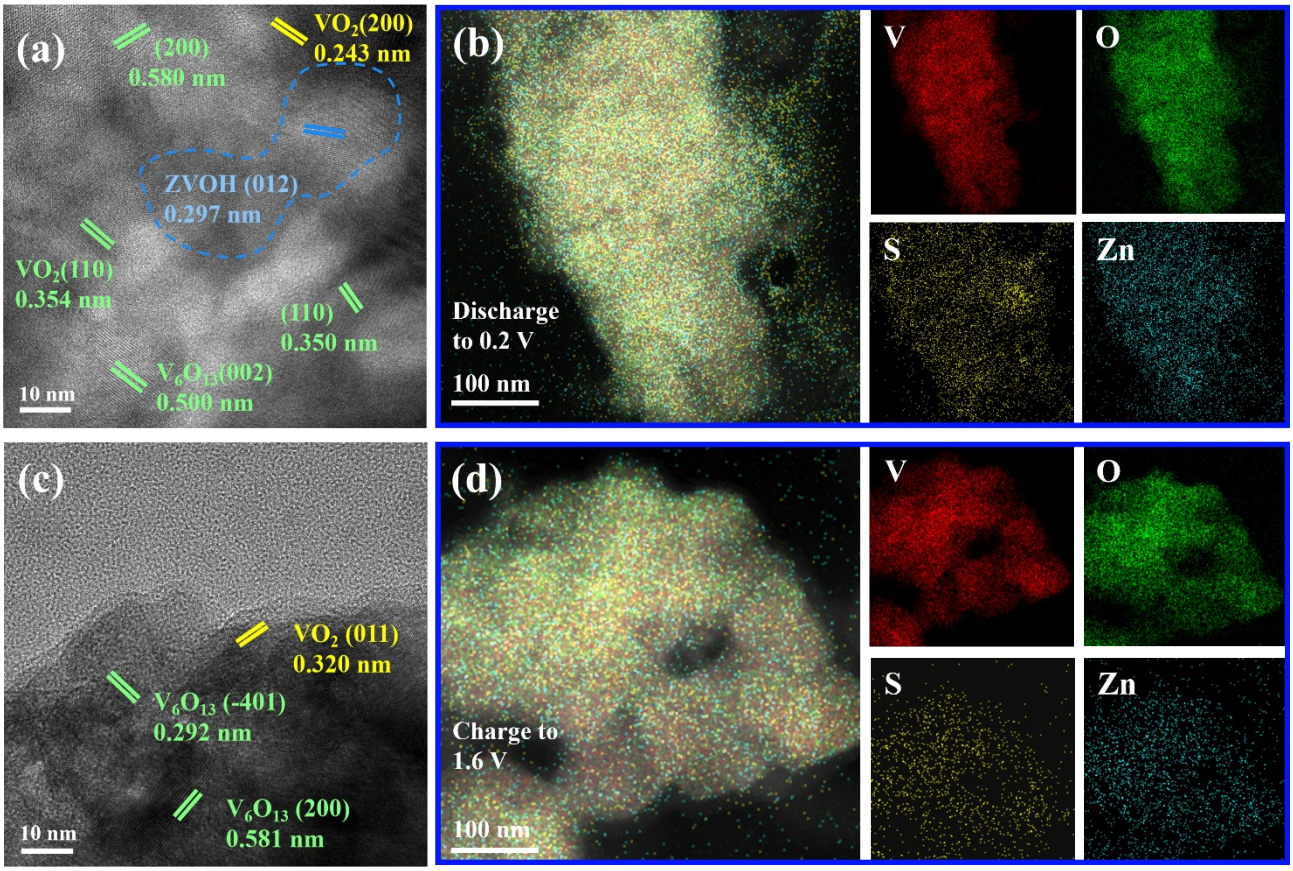

Figure S8. Ex-situ TEM of SVO-2 electrode. HRTEM images and EDS images in fully (a, b) discharged and (c, d) charged states in the 2nd cycle.

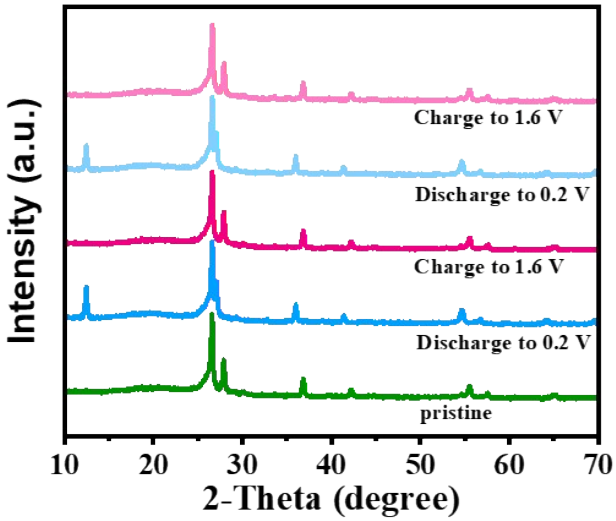

Figure S9. XRD curves of SVO-2 in fully charged-discharged states during different cycles.

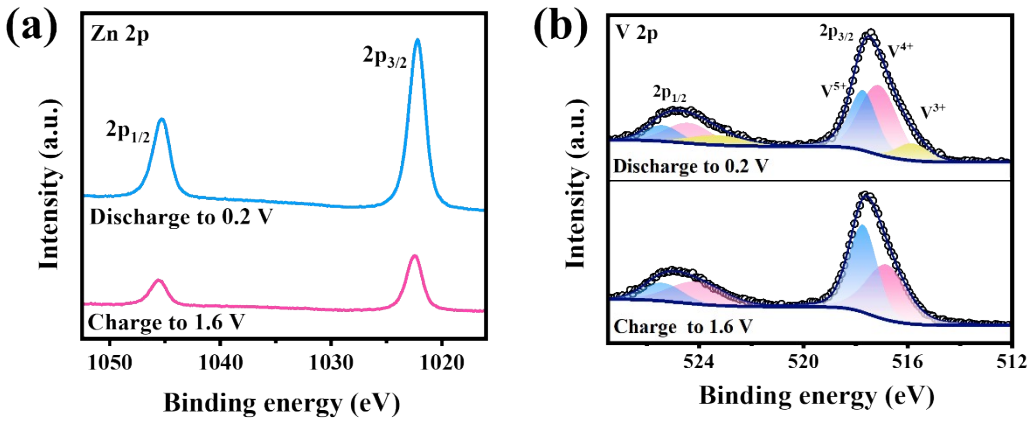

Figure S10. Ex-situ XPS spectra of Zn 2p and V 2p regions in fully discharged and charged states of SVO-2 electrode in the 2nd cycle.

Table S1. S contents of the SVO samples measured by ICP.

Samples	S (wt%)
SVO-1	0.1043
SVO-2	0.1031
SVO-3	0.0810
SVO-4	0.1194

References

1 G. Kresse, J. Furthmüller, *Comput. Mater. Sci*, 1996, **6**, 15-50.
2 G. Kresse, J. Furthmüller, *Phys. Rev. B*, 1996, **54**, 11169-11186.
3 J.P. Perdew, K. Burke, M. Ernzerhof, Phys. *Rev. Lett.*, 1996, **77**, 3865-3868.
4 G. Kresse, D. Joubert, *Phys. Rev. B*, 1999, **59**, 1758-1775.
5 P.E. Blöchl, *Phys. Rev. B*, 1994, **50**, 17953-17979.
6 S. Grimme, J. Antony, S. Ehrlich, H. Krieg, *J. Chem. Phys.*, 2010, **132**, 154104.
7. G. Henkelman, B.P. Uberuaga, H. Jónsson, *J. Chem. Phys.*, 2000, **113**, 9901-9904.